EURASIP Journal on Advances in Signal Processing

RESEARCH Open Access

Force estimation for human–robot interaction using electromyogram signals from varied arm postures

Thantip Sittiruk[1], Kiattisak Sengchuai[1], Apidet Booranawong[1], Paramin Neranon[2] and Pornchai Phukpattaranont[1*]

*Correspondence:
pornchai.p@psu.ac.th

[1] Department of Electrical and Biomedical Engineering, Faculty of Engineering, Prince of Songkla University, Hat Yai 90110, Songkhla, Thailand
[2] Department of Mechanical and Mechatronics Engineering, Faculty of Engineering, Prince of Songkla University, Hat Yai 90110, Songkhla, Thailand

Abstract

In this paper, a system for force estimation based on surface electromyography signals measured from the eight channels of the Myo armband is presented. We evaluated nineteen regression models to continuously estimate force in three scenario cases to cover the natural movement in two degrees of freedom planer rehabilitation mobile robots. The best estimation model that could overcome the challenge in a variety of different scenarios was determined. Based on the experimental results, the Gaussian process regression model performed best, giving a root mean square error in the overall range of 1.18–1.77 N. Additionally, the results showed that the exponential algorithm outperformed other solutions, significantly reducing the force estimation error.

Keywords: sEMG, Force estimation, Regression models, Human–robot interaction

1 Introduction

Surface electromyography (sEMG) can be applied in a wide variety of human–robot interaction applications, including motion classification, joint angle prediction, and force estimation. Firstly, with just two pairs of active surface electrodes on each forearm, twenty-five robotic commands can be controlled in real time in a robotic arm [1]. Secondly, recent research on applications of sEMG for joint angle prediction includes the determination of ground reaction forces and lower body joint angles from sEMG sensors during a step-down task for people with osteoarthritis [2], continuous prediction of joint angle from sEMG via a multi-feature temporal convolutional attention network [3], and prediction of the finger angle position of the first joint based on the value of the forearm's sEMG and the finger's previous location [4]. Thirdly, muscle force estimation is essential for biomechanical modelling and natural human–machine interaction. Estimating the muscle forces of the human arm has also been explored [5, 6], with applications in prosthetic control and rehabilitation robots [7–11]. Muscle contractions produce forces and enable humans to move. The forces generated by muscles in response

to brain control signals are dependent on an immense number of variables dispersed over several spatiotemporal scales [12], making muscle force prediction challenging [13].

Force sensors are in charge of measuring the force exerted on an object. Tensile and pressure forces, in general, do not require sensors to directly estimate muscle forces due to the cost and size of the sensor. In addition, muscle activity can be monitored by recording either the relevant electrical or mechanical phenomena [14]. Surface electromyography (sEMG) is the total of subcutaneous motor action potentials generated by muscle contraction [15], which can represent neuromuscular activity. The sEMG can be used to assess the patient's voluntary effort. Moreover, the brain drive to the muscle is detected by sEMG [16–18]. It is feasible to estimate muscle force production by modelling the association between brain control signals and muscle force using knowledge of the neurological system because muscle contraction causes joint forces to be produced. Many rehabilitation devices are controlled by sEMG signals, which are generated by the electrophysiological and mechanical activations of muscles [19, 20]. The relationship between sEMG and muscle force has been the subject of research for various applications due to its ease of collection and non-invasiveness.

The study of the relationship between sEMG and force is varied and growing in this field. There are mathematical model-based approaches with complex parameters that rely on specific muscle information [21–25]. Furthermore, a machine learning technique has been utilized to develop a nonlinear relationship between sEMG and force. A review of related works presented in the literature has been described below.

A deep convolutional neural network (CNN) based on a regression model was introduced in [5, 13, 26]. To estimate the contract force at the wrist for sophisticated inter-subject force modelling during isometric elbow flexion contractions [5], models with feature-level fusion of the sEMG in both time and frequency domains were used. Furthermore, in [14], five deep convolutional modules were proposed to map the interaction force and sEMG signals when hand contact emerged directly on the robot's arm, which worked in the desired Cartesian location for the task of physical human–robot interaction. To improve the middle hidden layer [26], the constrained autoencoder network (CAEN) was proposed to improve extracting features with reduced dimensions. Such a suggested model was also compared for effectiveness with four models in an artificial neural network for estimating simultaneous finger activity as well as the impact of human engagement in actual prosthetic hand control.

In [15], they compared several types of neural networks and selected the method that provided the best performance. A real-time estimate in perpendicular degrees of freedom (DoFs) was accompanied by task force, such as tightening or loosening a screwdriver (restricted motion). A long short-term memory (LSTM) network was presented in natural human–robot interaction (HRI) for the simultaneous estimation of motion and interaction force. In [21], the gripping force for object-grabbing in the three-finger pinch mode was estimated from sEMG signals. To achieve a rapid and precise prosthetic hand, various types of neural networks, including basic recurrent neural networks (RNN), long short-term memory (LSTM), gated recurrent units (GRU), and multilayer perceptron networks (MLP), were employed. For the study in [16], high-density sEMG signals were analyzed for time and frequency domain features (336 features from 21 channels) in order to create nonlinear bagged tree ensemble

(BTE) models for isometric force estimation. Finally, [27] presented an approach for myoelectric control systems based on multivariable system identification in state space (SS). The Kalman filter was also applied for proportional and continuous grasping force estimation. The main purpose was to describe a new approach for predicting gripping force in real time using sEMG measurements in order to control a hand prosthesis.

A summary of related works, with a special focus on force estimation tested in the muscle area of the human arm, hardware, experimental setups and force patterns, force estimation models, and objectives based on sEMG signals, is also provided in Table 1.

According to the literature survey introduced above, in this paper, we propose a muscular force estimation based on sEMG signals. The aims and contributions of this work are fourfold.

- First, a system for forearm muscle estimation based on sEMG signals measured from the Myo armband is presented. A force sensor is installed on a mobile robot, with a handle on the sensor so that force can be applied according to the movement pattern in the XY plane.
- Second, in order to cover the format for actual physical estimation, we consider force patterns covering axial movements in the two-dimensional plane, and elbow placement in three scenarios in fixed and free positioning is studied.
- Third, nineteen regression models are applied and evaluated, including: Gaussian process regression (GPR) with rational quadratic, exponential, squared exponential, and matern 5/2 kernels; neural networks (NN) with different layers, namely narrow, medium, wide, bilayered, and trilayered; linear regression (LR) with linear, robust, stepwise, and interactions models; and support vector machines (SVM) with quadratic, medium Gaussian, linear, coarse, cubic, and fine Gaussian kernels.
- Finally, regression models' performances are validated with various test scenarios based on the design of force patterns. The evaluation is considered based on root mean square error (RMSE) values, speeds, and times required to achieve a model. Our major findings indicate that the GPR model with the exponential algorithm obtains the best results with the RMSE in the range of 1.18–1.77 N. The model can potentially be used to estimate the force of a mobile robot in two planes, and it is capable of estimating forces close to the force recorded from the force sensor.

The structure of this paper is as follows. The methodology, which consists of a data acquisition and experimental protocol, test scenarios, force estimation, and regression models, is included in Sect. 2. In Sect. 3, results, signal characteristics, performance comparison, and signal comparison are given. Finally, we discuss and conclude the paper in Sect. 4.

2 Methodology

2.1 Data acquisition system and experimental protocol

The data acquisition system was designed to simultaneously collect sEMG and force signals, as shown in Fig. 1. On the one hand, eight channels of sEMG signals were acquired from the Myo armband (Thalmic Labs, Kitchener-Waterloo, Canada), which is capable of transmitting 8-bit resolution data across wireless communication

Table 1 A summary of the related works

Ref./Year	Muscles	Hardware	Experimental setup	Force estimation algorithms	Objectives
[5]	Forearm	HD-electrode (21 channels) ATI 6-DOF Gramma force sensor (a single DOF)	Three isometric elbow flexions (60, 90, and 120 degrees) with three force levels of 20, 35, and 50% MVC The shoulder and wrist were held in a fixed position to constrain the elbow motion	CNN with feature-level fusion method (CNN-FLF) Compared with BTE, decision tree, LR, and SVM NMSE of $1.60 \pm 3.69\%$	Modelling inter-subject force during isometric contractions
[13]	Forearm	Myo armband (8 channels) 6-axis force sensor (3-DOF)	Three-hand movements in up-down, left–right, and front-back move the end of the robot The forearm is placed on the box at a level with the wrist	Deep convolutional neural network (DCNN) Compared with LSTM, single-layer neural networks (SNN), and multiple-layers neural networks (MNN) The mean square error (MSE) was 0.03, 0.01, and 0.04 for up-down, left–right, and front-back	Estimation of robot arm-hand interaction force in human–robot interaction
[15]	Upper arm and forearm	sEMG electrodes (6 channels) P200, SX230-1000 Biometrics (a single DOF)	Three force levels (small, medium, and large forces) Subjects grasped the handle with the forearm parallel to the shaft axis and the upper arm perpendicular to the forearm	Long short-term memory (LSTM) Compared with artificial neural networks (ANN) Root mean square error (RMSE) was in the range of 3.82 ± 0.74 N	Mimicking confined actions with a screwdriver, such as tightening or loosening a screw
[16]	Upper arm and forearm	HD-EMG (21 channels) ATI 6-DOF Gramma force sensor (a single DOF)	Three joint angles (60, 90, and 120 degrees), three force levels (20, 35, and 50% MVC), and two forearm postures induced force at the wrist Force was measured at the wrist and at the elbow placed in the same plane	Bagged tree ensemble (BTE) model Compared with decision trees, linear regression (LR), and support vector machines (SVM) Average normalized mean squared error (%NMSE) of $5.65 \pm 16.24\%$	The isometric force estimate model produced a more general
[21]	Forearm	Myo armband (8 channels) ATI 6-axis (mini45 series) force sensor (a single DOF)	The force of the three-finger pinch grip was simultaneously measured at the maximum force level The hand and forearm positions were on the table, and the elbow and wrist angles were 0 and 90 degrees in a fixed arm position	Gated recurrent units (GRU) Compared with neural networks (multilayer perceptron (MLP)), simple recurrent neural networks (RNN), and LSTM Mean square error (MSE) was 0.005	The three-finger pinch mode's gripping force

Table 1 (continued)

Ref./Year	Muscles	Hardware	Experimental setup	Force estimation algorithms	Objectives
[26]	Forearm	Bipolar sensor electrode (12 channels) Load cell (a single DOF)	Fingers moved by profiling a sine function (a minimum value is zero, and a maximum value is one) The arm restraint system consisted of a handgrip, a wrist rest, and an elbow rest	Constrained autoencoder network (CAEN) Compared with ANN, non-negative matrix factorization (NMF), common spatial pattern (CSP), and NMF with Hadamard product (NMF-HP) Average RMSE of around 0.17	The simultaneous and proportional force of the fingers (thumb, index, and middle fingers) was estimated
[27]	Forearm	Myo armband (8 channels) Force sensitive resistor (FSR) (a single DOF)	Grasping force on a ball is measured at three levels: small, medium, and high forces The wrist and elbow are on the same plane	Recursive least squares (RLS) algorithm in a state-space model with a Kalman filter (SS-KF) Compared with the MLP network, recurrent nonlinear autoregressive exogenous (NARX), and linear discriminant analysis (LDA) NRMSE was 0.72 ± 0.06	A model for estimating proportional and continuous gripping force in order to develop a robotic hand
[28]	Forearm	Myo armband (8 channels) Load cell (2-DOF)	Four movements (wrist flexion, extension, radial deviation, and ulnar deviation) The forearm was fixed, and the height of the support coincides with the bottom of the handle	ANN for fatigue classification	Patients with strokes generate wrist movements with their impaired arms
This work	Forearm	Myo armband (8 channels) ATI 6-axis force sensor (2-DOF)	Four movements in the XY plane of directions, along with the x and y axes in positive and negative Three scenario cases with different heights of the elbow (fixed to the table and box, and free)	Gaussian process regression (GPR) Compared with NN, LR, and SVM The average RMSE of the GPR in scenarios 1, 2, and 3 was 1.32 ± 0.02, 1.62 ± 0.20, and 2.00 ± 0.88 N	Model estimation by sEMG in the 2-DOF plane

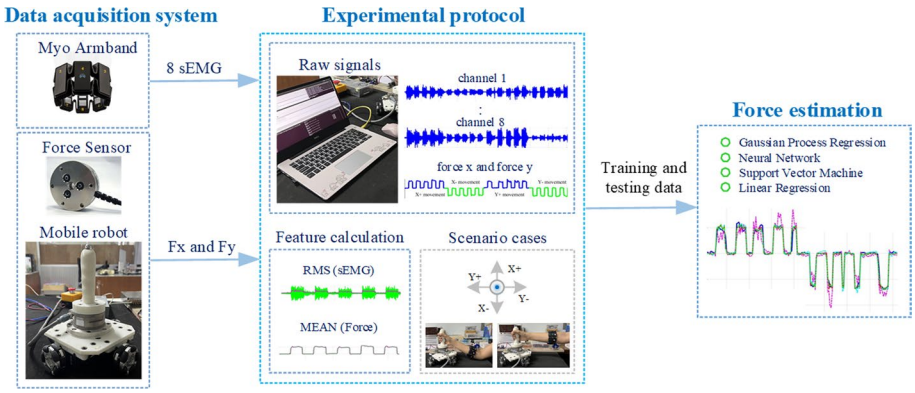

Fig. 1 A block diagram of the overall system

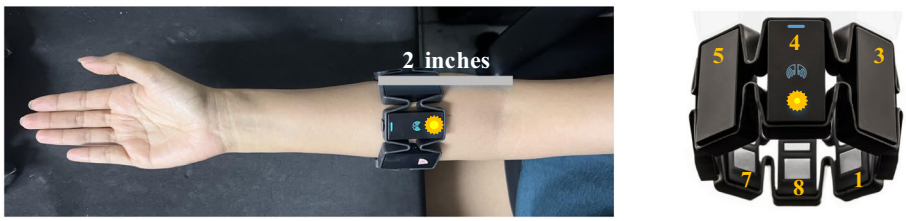

Fig. 2 A placement of the Myo armband on the forearm

via Bluetooth protocol. On the other hand, the 6-axis force and torque sensor (ATI: Mini40), which was placed at the base of a mobile robot, was utilized to measure the force signals in the X and Y axes. The mobile robot is composed of four wheels. The handle was designed to push the mobile robot to move in the XY plane. However, in this experimental setup, the mobile robot was fixed (not moving). A sampling rate of 200 Hz was used for both EMG and force signal collections.

In the experiment, there were two participants (34 ± 1 years, 1 male and 1 female). The experiments were in accordance with the Declaration of Helsinki. Before data collection, all participants were informed of the experimental protocols so that they were familiar with the setup and the procedure and agreed to participate in the test. The signals were collected based on ROS Kinetic, operating under Ubuntu and running Python for real-time visualization and data storage. The Myo armband was placed on the forearm, approximately 2 inches from the elbow. A reference channel was fixed at the yellow dot shown in Fig. 2, which matched the fourth channel of the Myo armband. The corresponding muscle to this sEMG channel was the pronator teres. The location of the other seven channels and their corresponding muscles is shown in Table 2.

In the experimental setup, force signals from four directions of wrist movements, namely, the positive X-, negative X-, positive Y-, and negative Y-axes, were collected. The movement sequence was shown in Fig. 3. In each direction, there were ten sessions of movements. In each session, the participant alternately took a rest and exerted force for 10 s each. In total, each direction was performed for 20 s. The number of samples for each channel of the sEMG signal and a force signal was 40,000

Table 2 Distribution of the sEMG electrodes on the forearm

EMG channel	Muscle
1	Extensor Digitorum Cummunis
2	Extensor Carpi Radialis
3	Brachioradialis
4	Pronator Teres
5	Flexor Carpi Radialis
6	Flexor Carpi Ulnaris
7	Flexor Digitorum
8	Extensor Carpi Ulnaris

Fig. 3 The movement sequence used for collecting sEMG and force signals from four directions

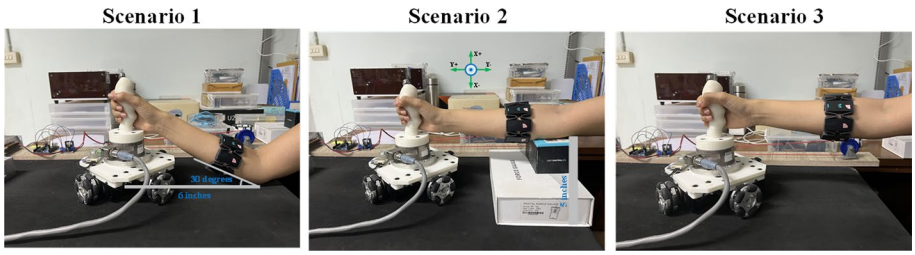

Fig. 4 The scenario cases in the experimental setup. (Left) The elbow position was fixed at an angle of 30 degrees to the floor. (Middle) The elbow position was fixed and parallel to the floor. (Right) The elbow position was free

(20 s × 200 Hz). To avoid fatigue, there was a one-minute rest between each direction of movement. The number of samples collected from all four directions was 160,000 (40,000 samples × 4 directions). Furthermore, the experiment was done twice, with identical protocols for each of the four directions of movement.

2.2 Test scenarios

The participant sat comfortably in a chair in front of a computer screen for signal visualization and grasped the handle when the forearm was held in place to prevent needless wrist bending. The participant then performed three different test scenarios where the elbow was placed in different positions during isometric contractions, as shown in Fig. 4. The details of each scenario are as follows.

2.2.1 Scenario 1

The elbow position was fixed on the floor at a distance of 6 inches from the device, and the lower arm is at an angle of 30 degrees to the floor, as shown in Fig. 4 (Left).

This type of experimental setup provided the muscle force in the case of isometric movement.

2.2.2 Scenario 2

The elbow position was fixed and parallel to the floor. In this scenario, the elbow was placed on the box at a height of 5 inches, as shown in Fig. 4 (Middle). Most experimental setups for force estimation using sEMG signals from previous publications used this scenario.

2.2.3 Scenarios 3

The elbow position was free, and it was approximately parallel to the floor, as shown in Fig. 4 (Right). The sEMG and force signals collected from this scenario were close to the natural movement along each direction compared to scenarios 1 and 2.

2.3 Force estimation

There were three steps in force estimation: segmentation, feature calculation, and regression. The details of each step are as follows.

2.3.1 Step (1) segmentation

After sEMG and force signals were collected, they were divided into small segments using a window without overlapping. The window length was 50 samples (250 ms). As a result, for the data collected from the movement in each direction, the number of segments from each channel of the sEMG signal and a force signal was 800 (40,000 samples/50 samples per segment).

2.3.2 Step (2) feature calculation

The segmented data from Step (1) was used for calculating features in this step. The root mean square (RMS) value is used as a feature for sEMG signals, which can be expressed as

$$\mathrm{RMS}_k^m = \sqrt{\frac{1}{N}\sum_{i=1}^{N} x_i^2} \tag{1}$$

where x_i is the amplitude of the sEMG sample in the segment, N is 50, k is the segment number, and m is the sEMG channel number ($1 \leq m \leq 8$). For the force signal, the mean (MEAN) value is used as a feature, which is given by

$$\mathrm{MEAN}_k = \frac{1}{N}\sum_{i=1}^{N} f_i \tag{2}$$

where f_i is the force sample in the segment.

Table 3 NN models' architecture and parameters

Parameters	Narrow	Medium	Wide	Bilayered	Trilayered
Number layers	1	1	1	2	3
First layer size	10	25	100	10	10
Second layer size	–	–	–	10	10
Third layer size	–	–	–	–	10
Activation	ReLU	ReLU	ReLU	ReLU	ReLU
Iteration limit	1000	1000	1000	1000	1000

Table 4 SVM models' hyperparameters

Parameters	Linear	Quadratic	Cubic	Fine	Medium	Coarse
Kernel function	Linear	Quadratic	Cubic	Gaussian	Gaussian	Gaussian
Kernel scale	Automatic	Automatic	Automatic	0.71	2.80	11.00

2.3.3 Step (3) Regression

In this step, the RMS and MEAN features from Step (2) are used to train a regression model for estimating force from the sEMG signals. In model training, while the *RMS* features from 8-channel sEMG signals are formed as an input vector for the regression model, the *MEAN* features from the force signal are formed as an output vector. For example, there are 800 feature values per channel in the movement from each direction and scenario. Then, the number of features 640 is used for model training and validation, and the number of features 160 is used for model testing. In addition, fivefold cross-validation is used for the training model.

2.4 Regression models

This research compares and tests four regression models: Gaussian process regression (GPR), neural networks (NN), linear regression (LR), and support vector machines (SVM). The following provides a brief overview of each regression model and the associated parameters that were used:

GPR integrates latent variables and an explicit basis function for describing the target [29–31]. Four kernels of the GPR model were utilized in this study, namely rational quadratic, exponential, squared exponential, and matern 5/2.

NN used in this paper employs a feedforward in a multilayer perceptron network architecture. Five NN regressions are studied, namely narrow, medium, wide, bilayered, and trilayered [32]. The network architecture only includes one layer for narrow, medium, and wide NNs. Meanwhile, bilayered and trilayered network architectures have two and three layers, respectively. The ReLU activation function is used in the model to conduct a threshold operation on each element of the input, where any value less than zero is set to zero. The learning algorithm is the Levenberg–Marquardt algorithm. More details on the NN parameters are shown in Table 3.

LR assumes a linear relationship between the output and the input of the regression model [30, 33]. Multiple linear regression is a generalization of simple linear regression

with more than one independent variable and a subset of general linear models with only one dependent variable.

SVM works by translating the data from its original space into a higher-dimensional one, which is known as the feature space, by a mapping function [30, 34]. In this work, six forms of SVM regression are used, namely linear, quadratic, cubic, fine Gaussian, medium Gaussian, and coarse Gaussian. More details on the SVM parameters are shown in Table 4. We note that to obtain the optimal NN and SVM models, hyperparameter optimization through a grid search or a random search algorithm should be considered to find the best estimation result.

2.5 Performance evaluation

In the training and testing steps, the major metric for evaluating the performance of each regression model was the root mean square error (RMSE), which can be expressed as

$$\mathrm{RMSE} = \sqrt{\frac{1}{M}\sum_{i=1}^{M}(\hat{F}_i - F_i)^2} \tag{3}$$

where M is the number of force samples, $\hat{F}_i$ is the estimated force, and F_i is the measured force. In order to compare the performance of the proposed method to those from previous publications, other metrics are calculated, including normalize mean square error (NMSE), normalize root mean square error (NRMSE), and mean absolute error (MAE), which are given by

$$\mathrm{NMSE} = \frac{\sum_{i=1}^{M}(\hat{F}_i - F_i)^2}{\sum_{i=1}^{M}F_i^2} \tag{4}$$

$$\mathrm{NRMSE} = 1 - \frac{\mathrm{RMSE}}{\sqrt{\sum_{i=1}^{M}(\hat{F}_i - F_i)^2}} \tag{5}$$

$$\mathrm{MAE} = \frac{1}{M}\sum_{i=1}^{M}\left|\hat{F}_i - F_i\right| \tag{6}$$

Force estimation from all scenarios in this paper were run on a computer using an Intel$^{(R)}$Core$^{™}$ i7-8565U@1.80 GHz processor with 8 GB of RAM.

3 Results

3.1 Signals characteristics

Figure 5 shows an example of five sessions of 8-channel sEMG and force signals for four directions of movement in scenario 1 from subject 1. The Myo armband collects these sEMG signals with an 8-bit resolution ranging from − 128 to 127. The amplitude and direction of the force pattern on the X and Y axes are recorded from the force sensor. The results indicate that the difference in movement direction provides different patterns among 8-channel sEMG signals, which are caused by the contraction of different muscle groups.

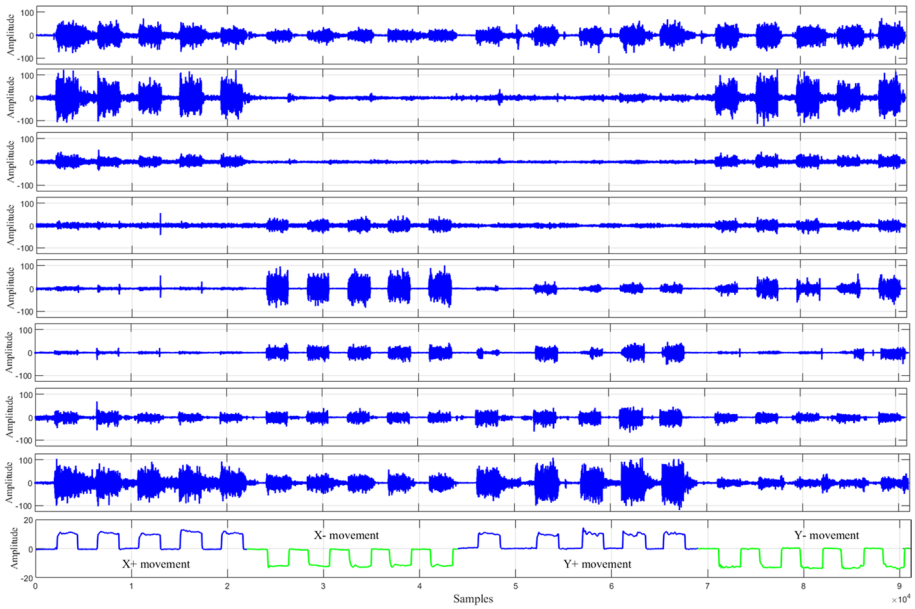

Fig. 5 Examples of measured 8-channel sEMG and force signals for four directions of movement in scenario 1 from subject 1

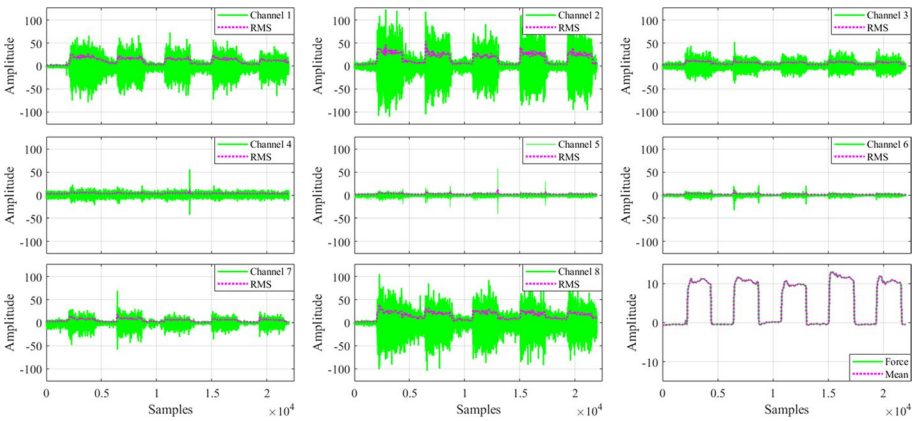

Fig. 6 Examples of RMS and MEAN features for positive X movements in scenario 1 from subject 1

From the collected 8-channel sEMG and force signals, the RMS and MEAN features are determined. Examples of RMS and MEAN features for the positive X movements in scenario 1 from subject 1 are shown in Fig. 6 with a pink line.

3.2 Performance comparison

After RMS and MEAN features are extracted, the force is estimated by the proposed four regression models, namely GPR, NN, LR, and SVM. The RMSE values from the four regression models in scenario 1 are shown in Fig. 7, where the best algorithm for each model is shown. The performance indices defined in the training and testing phases are shown as the mean and standard deviation of RMSE values averaged across 5-folds for each scenario case of all movement patterns.

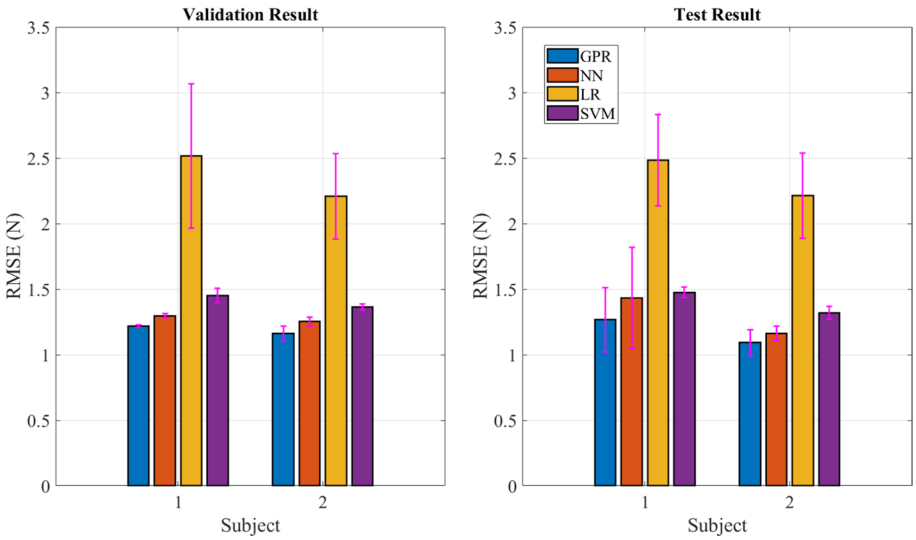

Fig. 7 RMSE values from the four regression models in scenario 1

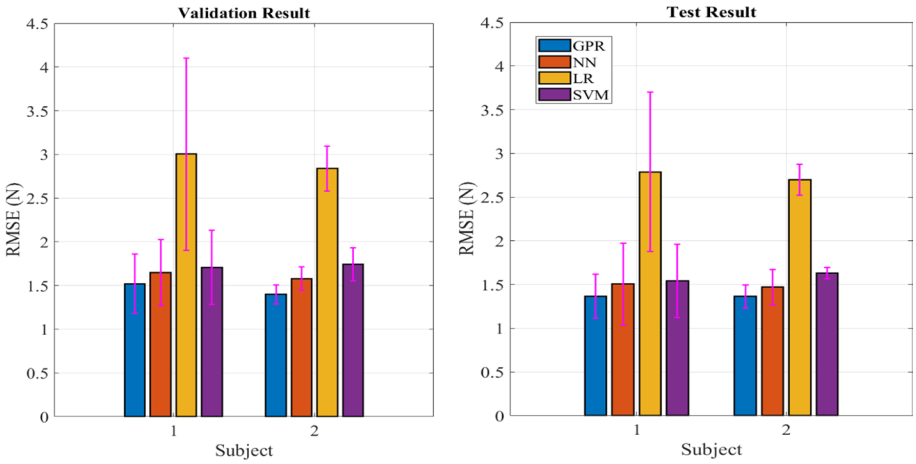

Fig. 8 RMSE values from the four regression models in scenario 2

It has been discovered that GPR provides the best overall force estimating accuracy among both training and testing of all subjects. NN and SVM give decent accuracy but are less accurate than GPR, while LR has the least approximation ability. In the case of subject 2, the error results for all models are significantly higher than in the case of subject 1. As a consequence, based on the average RMSE values of 1.267 and 1.093 N in the average of force estimation from scenario 1, the results show that the GPR is the best estimate model, followed by NN and SVM, respectively.

Figure 8 shows the RMSE values from the four regression models in scenario 2. In terms of the RMSE values from the same exertion pattern, it is discovered that the overall error values from all four models in scenario 2 are higher than those in scenario 1. The GPR model gives the force-estimating abilities of RMSE in the ranges of 1.363–1.520 N. Furthermore, while NN and SVM produce similar force-estimating results in subject 1, the LR model as a whole produces rather high error amounts when compared to the

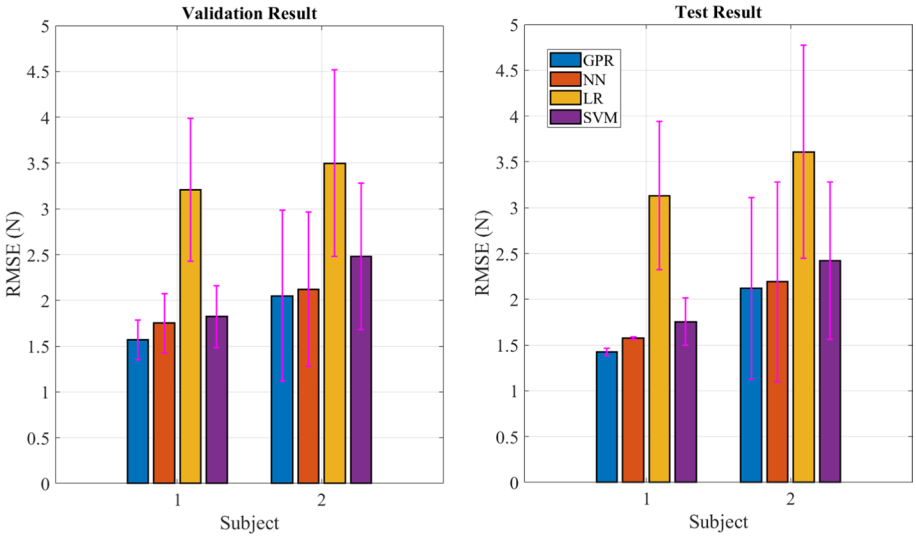

Fig. 9 RMSE values from the four regression models in scenario 3

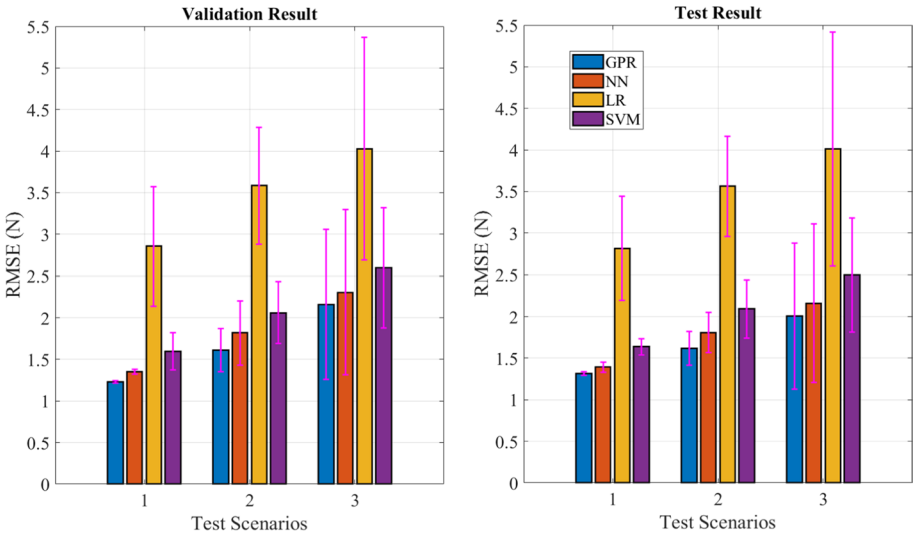

Fig. 10 RMSE values from the four regression models of two subjects

three models mentioned above. As a result, in scenario 2, the GPR model overtakes the NN and SVM models in terms of accuracy of force estimation.

The RMSE values from the four regression models in scenario 3 are shown in Fig. 9. In terms of the RMSE efficiency from the same exertion pattern, it is discovered that the overall error values from all four models in scenario 3 are higher than those from scenarios 1 and 2 because the elbow is free in this scenario. When comparing subject 1 to subject 2, the four models' force-estimating error is smaller in subject 1. The NN and SVM models outperform the LR in terms of force estimation. However, for force estimation in Scenario 3, the GPR model still produces lower error values than the NN and SVM models do.

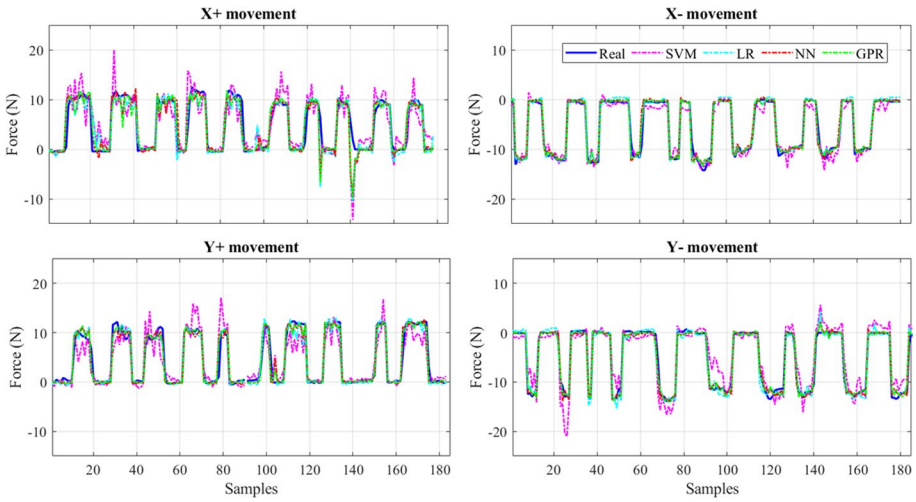

Fig. 11 Comparison of the estimated forces from four regression models with the measured force in scenario 1

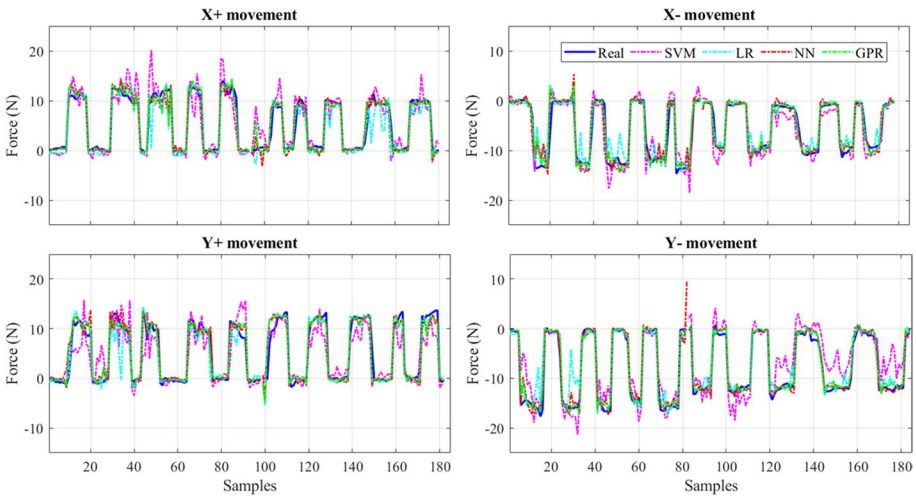

Fig. 12 Comparison of the estimated forces from four regression models with the measured force in scenario 3

When the data from both subjects is used in both training and testing steps, the RMSE values from all scenarios are shown in Fig. 10. The RMSE values from scenario 1 are lower than those from scenarios 2 and 3 because they are estimated by the sEMG and force signals collected when the elbow is fixed on the table. On the other hand, the RMSE values from scenario 3 are the highest. Moreover, the GPR model with an exponential algorithm yields the lowest RMSE for all three scenarios, whereas the LR model with an interaction algorithm gives the highest RMSE.

4 Discussion

4.1 Signal comparison

The estimated forces from four regression models, namely GPR, NN, LR, and SVM, are shown in Figures 11 and 12 with green, red, cyan, and pink lines, respectively, compared to the measured force in the blue line. The algorithm with the best results is chosen to estimate the muscular force of the four models (details of the algorithm from the testing results are presented in Fig. 10). The graph's details include exerting force in four ways: moving along the positive axes X and Y and the negative axes X and Y of subjects 1 (signal waveforms 1 to 5) and 2 (signal waveforms 6 to 10), respectively.

In scenario 1, the GPR model estimates force accurately across the whole range of force exerted in a negative direction on both the X and Y axes (X-movement and Y-movement) and a positive direction ($X+$ movement and $Y+$ movement), as shown in Fig. 11. The force estimation from the GPR model is better than that the other three models. The LR model estimates force with the lowest accuracy in all directions of movement. The NN and SVM models are found to be more accurate and have near-maximal force estimation accuracy as compared to the actual force exertion.

The GPR model provides more accurate force estimation than the NN model in scenario 3, as shown in Fig. 12. However, both models have near-optimal force prediction accuracy in all cases of pushing directions. The force estimation results for the SVM model are slightly better than those for the LR model, but they are still worse than the GPR and NN models. When looking at the overall picture in both the positive and negative directions, it can be concluded that the GPR model has a comparatively good force estimation ability when compared to the other three models. Force estimation from four regression models in scenario 3 is shown to be less accurate than those from scenario 1.

4.2 Performance comparison

The RMSE values from the four regression models in scenarios 1 to 3 for subjects 1 and 2, as shown in Figs. 7, 8 and 9, demonstrate a consistent trend. Furthermore, when data from both subjects is used in both the training and testing steps, the RMSE values from all scenarios shown in Fig. 10 also exhibit a similar trend. Specifically, GPR achieves the lowest RMSE value, while LR has the highest RMSE value. These results indicate a promising direction and suggest the potential for applying the proposed method to individuals of varying ages. However, further data acquisition and analysis are necessary to validate this assumption, which will be a focus of future research.

To address muscle fatigue, we designed a data collection protocol that minimizes its impact. Each participant completed ten sessions of movements in each direction, with each session consisting of alternating periods of rest and exertion lasting 10 s each. Between movements in different directions, participants rested for one minute. We also experimentally determined the median frequency of sEMG signals from channel 1 when the subject exerted force in the $X+$ direction. The mean and standard deviation of this median frequency were 69.4 Hz and 1.2 Hz, respectively. The results showed no significant decrease in the median frequency, indicating that muscle fatigue was not present.

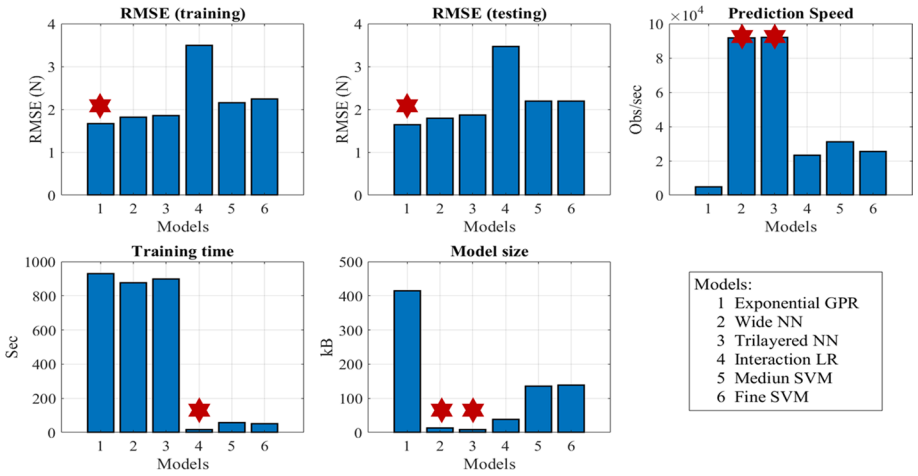

Fig. 13 Comparison of the best regression models in terms of computations

4.3 Computation complexity

Figure 13 summarizes model performance in terms of prediction speed, training time, and model size. In detail, it is discovered that there are only algorithms from the GPR model and the NN model that give force estimation results with the least error from both training and testing steps. When considering LR and SVM compared to GPR and NN, they have a higher force estimation error. When it comes to prediction speed, it has been discovered that both structures of the NN model have better prediction speed than the GPR model does, particularly the wide and the trilayered. In terms of training time, the GPR and NN models require roughly the same amount of time. The GPR model has a reserved model size of 415 kB for each algorithm, which is fairly high in comparison to the NN model. Therefore, it is possible to conclude that the GPR model with an exponential algorithm is appropriate for estimating force estimation based on sEMG in the XY plane.

5 Conclusions

In this paper, we propose four regression models, specifically GPR, NN, LR, and SVM, for estimating the muscle force based on sEMG signals that covered the X- and Y-axis movement patterns in three scenario cases where the combined elbow positions were fixed and free. The performances of these four models are compared based on the average RMSE values. The superiority of the GPR model with the exponential algorithm in scenarios 1 to 3 provides the RMSE values of 1.18, $\pm$ 0.17, 1.37 $\pm$ 0.19, and 1.77 $\pm$ 0.51 N, respectively. The RMSE from scenario 3 is the highest because the free elbow position causes more variation in sEMG signals. The model proposed in this paper can be utilized for estimating the force of a mobile robot in two planes and is capable of estimating forces that are close to the force recorded from the force sensor.

In future work, we will verify to guarantee the prediction accuracy of the dynamic force with more subjects and expect that this model with the highest performance will be a general model that can be easily applied and will be employed in real-time force estimation in practical applications.

Acknowledgements
This research was supported by National Science, Research and Innovation Fund (NSRF) and Prince of Songkla University (Ref. No. ENG6701305S).

Author contributions
T.S., A.B., P.N., and P.P. helped in methodology, T.S., K.S., A.B., P.N., and P.P. done investigation, T.S., and K.S. helped in writing—original draft preparation, T.S., A.B., and P.P. helped in writing—review and editing, T.S., K.S., A.B., and P.P. done supervision, A.B., P.N, and P.P.; All authors have read and agreed to the published version of the manuscript.

Funding
This research was supported by National Science, Research and Innovation Fund (NSRF) and Prince of Songkla University (Ref. No. ENG6701305S).

Availability of data and materials
No datasets were generated or analysed during the current study.

Declarations

Ethics approval and consent to participate
The analysis of the recorded data was conducted using completely anonymous data. The experimental study did not involve any invasive or medical procedures. All subjects gave their informed consent prior to the collection and acquisition of the data, which was carried out in compliance with the ethical principles of the Helsinki Declaration. Also, the participants, identities were kept confidential.

Consent for publication
All authors of this paper agree to publish the work in this paper.

Competing interests
The authors declare no competing interests.

Received: 13 March 2024 Accepted: 5 September 2024
Published online: 20 September 2024

References

1. R. Byfield, R. Weng, M. Miller, Y. Xie, J.-W. Su, J. Lin, Real-time classification of hand motions using electromyography collected from minimal electrodes for robotic control. Intent. J. Robot. Control **3**(1), 13–20 (2021). https://doi.org/10.5430/ijrc.v3n1p13
2. R. Byfield, M. Guess, K. Sattari, Y. Xie, T. Guess, J. Lin, Machine learning full 3-D lower-body kinematics and kinetics on patients with osteoarthritis from electromyography. Biomed. Eng. Adv. **5**, 100088 (2023). https://doi.org/10.1016/j.bea.2023.100088
3. S. Wang, H. Tang, L. Gao, Q. Tan, Continuous estimation of human joint angles from sEMG using a multi-feature temporal convolutional attention-based network. IEEE J. Biomed. Health Inform. **26**(11), 5461–5472 (2022). https://doi.org/10.1109/JBHI.2022.3198640
4. M. Vangi, C. Brogi, A. Topini, N. Secciani, A. Ridolfi, Enhancing sEMG-based finger motion prediction with CNN-LSTM regressors for controlling a hand exoskeleton. Machines **11**(7), 747 (2023). https://doi.org/10.3390/machines11070747
5. G. Hajian, A. Etemad, E. Morin, Generalized EMG-based isometric contact force estimation using a deep learning approach. Biomed. Signal Process. Control **70**, 103012 (2021). https://doi.org/10.1016/j.bspc.2021.103012
6. X. Yang, J. Yan, H. Liu, Comparative analysis of wearable A-mode ultrasound and sEMG for muscle-computer interface. IEEE Trans. Biomed. Eng. **67**(9), 2434–2442 (2019). https://doi.org/10.1109/TBME.2019.2962499
7. R. Gupta, I.S. Dhindsa, R. Agarwal, Continuous angular position estimation of human ankle during unconstrained locomotion. Biomed. Signal Process. Control **60**, 101968 (2020). https://doi.org/10.1016/j.bspc.2020.101968
8. I.J.R. Martinez, A. Mannini, F. Clemente, A.M. Sabatini, C. Cipriani, Grasp force estimation from the transient EMG using high-density surface recordings. J. Neural Eng. **17**(1), 016052 (2020). https://doi.org/10.1088/1741-2552/ab673f
9. H. Su, Y. Hu, H.R. Karimi, A. Knoll, G. Ferrigno, E.D. Momi, Improved recurrent neural network-based manipulator control with remote center of motion constraints: experimental results. Neural Netw. **131**, 291–299 (2020). https://doi.org/10.1016/j.neunet.2020.07.033
10. Y. Wang, B. Metcalfe, Y. Zhao, D. Zhang, An assistive system for upper limb motion combining functional electrical stimulation and robotic exoskeleton. IEEE Trans. Med. Robot. Bionics **2**(2), 260–268 (2020). https://doi.org/10.1109/TMRB.2020.2990318
11. A.S. Dhawan, B. Mukherjee, S. Patwardhan, N. Akhlaghi, G. Diao, G. Levay, R. Holley, W.M. Joiner, M. Harris-Love, S. Sikdar, Proprioceptive sonomyographic control: a novel method for intuitive and proportional control of multiple degrees-of-freedom for individuals with upper extremity limb loss. Sci. Rep. **9**(1), 9499 (2019). https://doi.org/10.1038/s41598-019-45459-7
12. G. Hajian, E. Morin, Deep multi-scale fusion of convolutional neural networks for EMG-based movement estimation. IEEE Trans. Neural Syst. Rehabil. Eng. **30**, 486–495 (2022). https://doi.org/10.1109/TNSRE.2022.3153252
13. H. Su, W. Qi, Z. Li, Z. Chen, G. Ferrigno, E.D. Momi, Deep neural network approach in EMG-based force estimation for human–robot interaction. IEEE Trans. Artif. Intell. **2**(5), 404–412 (2021). https://doi.org/10.1109/TAI.2021.3066565

14. W. Kuang, M. Yip, J. Zhang, Vibration-based multi-axis force sensing: design, characterization, and modeling. IEEE Robot. Autom. Lett. **5**(2), 3082–3089 (2020). https://doi.org/10.1109/LRA.2020.2975726
15. Q. Zhang, L. Fang, Q. Zhang, C. Xiong, Simultaneous estimation of joint angle and interaction force towards sEMG-driven human-robot interaction during constrained task. Neurocomputing **484**, 38–45 (2022). https://doi.org/10.1016/j.neucom.2021.05.113
16. G. Hajian, B. Behinaein, A. Etemad, E. Morin, Bagged tree ensemble modelling with feature selection for isometric EMG-based force estimation. Biomed. Signal Process. Control **78**, 104012 (2022). https://doi.org/10.1016/j.bspc.2022.104012
17. T. Chihara, J. Sakamoto, Exerted force estimation using a wearable sensor during manual material handling. Hum. Fact. Ergon. Manuf. Serv. Ind. **31**(3), 239–248 (2021). https://doi.org/10.1002/hfm.20881
18. Y. Li, W. Chen, H. Yang, J. Li, N. Zheng, Joint torque closed-loop estimation using NARX neural network based on sEMG signals. IEEE Access **8**, 213636–213646 (2020). https://doi.org/10.1109/ACCESS.2020.3039983
19. X. Jiang, B. Bardizbanian, C. Dai, W. Chen, E.A. Clancy, Data management for transfer learning approaches to elbow EMG-torque modeling. IEEE Trans. Biomed. Eng. **68**(8), 2592–2601 (2021). https://doi.org/10.1109/TBME.2021.3069961
20. G. Hajian, A. Etemad, E. Morin, Automated channel selection in high-density sEMG for improved force estimation. Sensors **20**(17), 4858 (2020). https://doi.org/10.3390/s20174858
21. A.G. Siavashani, A. Yousefi-Koma, A. Vedadi, Estimation and early prediction of grip force based on sEMG signals and deep recurrent neural networks. J. Braz. Soc. Mech. Sci. Eng. **45**(5), 264 (2023). https://doi.org/10.1007/s40430-023-04070-8
22. D. Xiong, D. Zhang, X. Zhao, Y. Zhao, Deep learning for EMG-based human-machine interaction: a review. IEEE/CAA J. Autom. Sin. **8**(3), 512–533 (2021). https://doi.org/10.1109/JAS.2021.1003865
23. H. Su, W. Qi, C. Yang, J. Sandoval, G. Ferrigno, E.D. Momi, Deep neural network approach in robot tool dynamics identification for bilateral teleoperation. IEEE Robot. Autom. Lett. **5**(2), 2943–2949 (2020). https://doi.org/10.1109/LRA.2020.2974445
24. C. Ma, C. Lin, O.W. Samuel, L. Xu, G. Li, Continuous estimation of upper limb joint angle from sEMG signals based on SCA-LSTM deep learning approach. Biomed. Signal Process. Control **61**, 102024 (2020). https://doi.org/10.1016/j.bspc.2020.102024
25. R. Ma, L. Zhang, G. Li, D. Jiang, S. Xu, D. Chen, Grasping force prediction based on sEMG signals. Alex. Eng. J. **59**(3), 1135–1147 (2020). https://doi.org/10.1016/j.aej.2020.01.007
26. Y. Cho, P. Kim, K.-S. Kim, Estimating simultaneous and proportional finger force intention based on sEMG using a constrained autoencoder. IEEE Access **8**, 138264–138276 (2020). https://doi.org/10.1109/ACCESS.2020.3012741
27. B. Dutra, A. Silveira, A. Pereira, Grasping force estimation using state-space model and Kalman Filter. Biomed. Signal Process. Control **70**, 103036 (2021). https://doi.org/10.1016/j.bspc.2021.103036
28. Y. Na, H. Lee, S. Kwon, Investigating the effects of long-term contractions on myoelectric recognition of wrist movements from stroke patients. Int. J. Precis. Eng. Manuf. **21**, 1771–1779 (2020). https://doi.org/10.1007/s12541-020-00364-2
29. X. Yang, J. Yan, Z. Chen, H. Ding, H. Liu, A proportional pattern recognition control scheme for wearable a-mode ultrasound sensing. IEEE Trans. Ind. Electron. **67**(1), 800–808 (2020). https://doi.org/10.1109/TIE.2019.2898614
30. A.T. Kamatham, M. Alzamani, A. Dockum, S. Sikdar, B. Mukherjee, Sparse sonomyography-based estimation of isometric force: a comparison of methods and features. IEEE Trans. Med. Robot. Bionics **4**(3), 821–829 (2022). https://doi.org/10.1109/TMRB.2022.3172680
31. J. Liang, Z. Shi, F. Zhu, W. Chen, X. Chen, Y. Li, Gaussian process autoregression for joint angle prediction based on sEMG signals. Front. Public Health **9**, 685596 (2021). https://doi.org/10.3389/fpubh.2021.685596
32. I. Chihi, L. Sidhom, E.N. Kamavuako, Hammerstein–wiener multimodel approach for fast and efficient muscle force estimation from EMG signals. Biosensors **12**(2), 117 (2022). https://doi.org/10.3390/bios12020117
33. Q. Zhang, A. Iyer, K. Kim, N. Sharma, Evaluation of non-invasive ankle joint effort prediction methods for use in neurorehabilitation using electromyography and ultrasound imaging. IEEE Trans. Biomed. Eng. **68**(3), 1044–1055 (2020). https://doi.org/10.1109/TBME.2020.3014861
34. S.-L. Lin, Application of machine learning to a medium Gaussian support vector machine in the diagnosis of motor bearing faults. Electronics **10**(18), 2266 (2021). https://doi.org/10.3390/electronics10182266

Publisher's Note